Temperature-driven transition from a semiconductor to a topological insulator

Steffen Wiedmann,[1,*] Andreas Jost,[1] Cornelius Thienel,[2] Christoph Brüne,[2] Philipp Leubner,[2] Hartmut Buhmann,[2] Laurens W. Molenkamp,[2] J. C. Maan,[1] and Uli Zeitler[1]

[1]*High Field Magnet Laboratory and Institute for Molecules and Materials, Radboud University, Toernooiveld 7, 6525 ED Nijmegen, The Netherlands.*

[2]*Physikalisches Institut (EP3), Universität Würzburg, Am Hubland, D-97074, Würzburg, Germany.*

(Received 19 November 2014; published 19 May 2015)

We report on a temperature-induced transition from a conventional semiconductor to a two-dimensional topological insulator investigated by means of magnetotransport experiments on HgTe/CdTe quantum well structures. At low temperatures, we are in the regime of the quantum spin Hall effect and observe an ambipolar quantized Hall resistance by tuning the Fermi energy through the bulk band gap. At room temperature, we find electron and hole conduction that can be described by a classical two-carrier model. Above the onset of quantized magnetotransport at low temperature, we observe a pronounced linear magnetoresistance that develops from a classical quadratic low-field magnetoresistance if electrons and holes coexist. Temperature-dependent bulk band structure calculations predict a transition from a conventional semiconductor to a topological insulator in the regime where the linear magnetoresistance occurs.

DOI: 10.1103/PhysRevB.91.205311 PACS number(s): 73.25.+i, 73.20.At, 73.43.−f

I. INTRODUCTION

Narrow-gap semiconductors possess conduction bands which are strongly non-parabolic and spin-orbit splittings that can be even larger than the fundamental band gap [1]. A particular interesting system is a type-III heterostructure composed of the semimetal HgTe and the wide-gap semiconductor HgCdTe with a low Hg content. These quantum well (QW) structures with an energy gap of several meV have already been experimentally investigated by means of optics and magnetotransport in the late 90s in order to obtain information about the band structure (BS) and the Landau level dispersion [2,3]. In 2006, Bernevig *et al.* predicted that the quantum spin Hall effect (QSHE) can be observed in inverted HgTe/CdTe QW structures if the layer thickness is larger than a critical value [4]. The system is then referred to as a two-dimensional (2D) topological insulator (TI) [5,6]. The hallmark of this state of matter is a quantized longitudinal conductance when the Fermi energy is in the bulk band gap and transport is governed by spin-polarized counter-propagating edge states. This quantized conductance has been found experimentally first in inverted HgTe QWs [7] and later on in InAs/GaSb heterostructures [8,9]. The existence of the helical states has been confirmed in inverted HgTe QWs by nonlocal measurements [10] and by verifying their spin polarization [11].

Bulk HgTe crystallizes in zincblende structure. When the semimetal HgTe with a negative energy gap of $E_g = -0.3$ eV is combined with the semiconductor HgCdTe, a type-III QW is formed. The band order in HgTe QWs with HgCdTe barriers depends strongly on the quantum confinement, i.e., the width d of the QW. For $d < d_c$, the system is a conventional direct band-gap semiconductor with a s-type Γ_6 conduction band and p-type Γ_8 valence band. d_c is the critical thickness of the QW where the system becomes a zero-gap semiconductor [12]. Calculations within the 8×8 $\mathbf{k} \cdot \mathbf{p}$ Kane model yield $d_c = 6.3$ nm for a QW on a $Cd_{0.96}Zn_{0.04}Te$ substrate and $d_c = 6.7$ nm on a CdTe substrate in the zero-temperature limit. For $d > d_c$ the BS is inverted, i.e., the $H1$ band is the conduction and the $E1$ band is the valence band, and the system is a 2D TI. Moreover, the system has an indirect band gap. If the well width is increased further, the confinement energy decreases and the system exhibits semimetallic behavior [13].

Apart from the variation of the QW thickness, temperature can induce a phase transition from a normal state ($T > T_c$) to a topologically nontrivial state of matter ($T < T_c$). This is caused by the strong temperature dependence of the $E1$ band, which is the topic of this paper. In order to provide experimental evidence for such a temperature-driven transition, we have performed magnetotransport experiments on four different HgTe quantum wells, all with a width exceeding the critical thickness d_c at $T = 0$. We show that we are in the regime of the QSHE and observe an ambipolar quantized Hall resistance at low temperature when the Fermi energy is tuned through the bulk band gap. In contrast, at room temperature we find electron and hole conduction that can be described by a classical two-carrier model. In an intermediate temperature range (100 K $\leqslant T \leqslant$ 205 K), where Shubnikov-de Haas oscillations and quantum Hall effect are absent, we observe a pronounced linear magnetoresistance (LMR) that develops from a classical quadratic low-field magnetoresistance (MR). Bulk band structure calculations using an eight-band $\mathbf{k} \cdot \mathbf{p}$ model demonstrate a transition from a conventional semiconductor to a topological insulator in the regime where the LMR is observed.

II. EXPERIMENTAL DETAILS AND SAMPLE CHARACTERIZATION AT $T = 4.2$ K

We have grown inverted HgTe QWs with (001) surface orientation by molecular beam epitaxy on a CdTe (sample S1, and S4) and on a $Cd_{0.96}Zn_{0.04}Te$ substrate (sample S2 and S3). Details for the samples S1–S4 are given in Table T1 in the supplemental material [14]. Lithographically defined Hall-bar structures have been produced with the dimension $(L \times W) = (600 \times 200)\ \mu m^2$. All samples are equipped with a metallic Au

*s.wiedmann@science.ru.nl

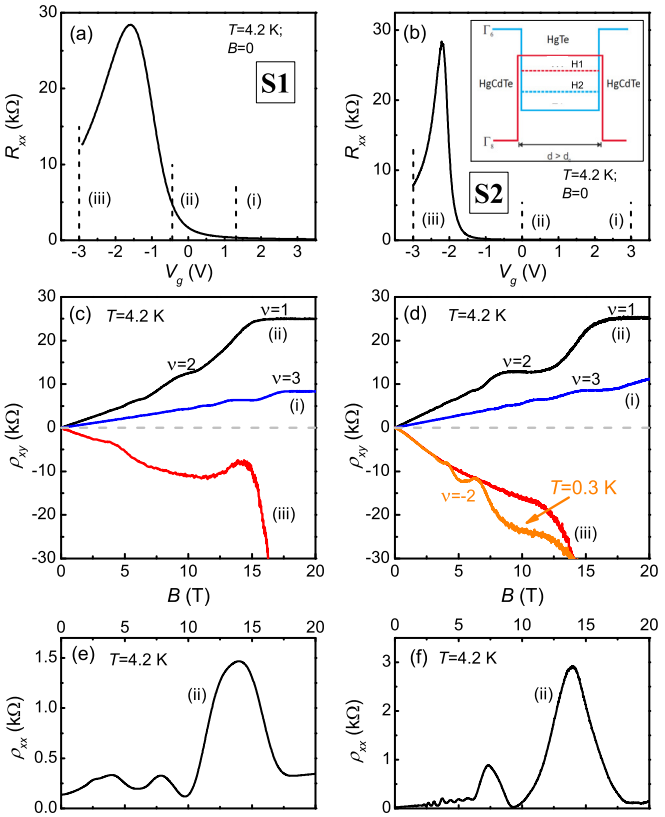

FIG. 1. (Color online) magnetotransport in the QSH regime for sample S1 and S2: Gate sweeps at $B = 0$ for samples S1 (a) and S2 (b). Panels (c) and (d) show the Hall resistivity $\rho_{xy}(B)$ for three gate voltage positions indicating the transition from electrons, in (i) and (ii), to holes in (iii). The inset in (b) sketches a HgTe type-III QW with inverted bands at $T = 4.2$ K. When the Fermi energy is in the bulk band gap, the $H2$ band is the valence band and the $H1$ band the conduction band.

top-gate, separated from the structure by an insulator made of a superlattice of Si_3N_4 and SiO_2, with a total thickness of 110 nm to tune the carrier concentration as a function of the applied gate voltage V_g. Four-probe measurements of longitudinal and transverse electrical resistances have been carried out using Stanford Research Systems SR830 Lock-In amplifiers with low constant voltage excitation. The samples were placed in a flow cryostat in a 33 T Bitter-type magnet.

In Fig. 1, we present transport at $T = 4.2$ K for sample S1 and sample S2 with a well width of $d = 12$ nm. Figures 1(a) and 1(b) show the longitudinal resistance R_{xx} at $T = 4.2$ K as a function of top-gate voltage V_g for samples S1 and S2. According to band structure calculations, both QWs are inverted at 4.2 K. The $H1$ band is the conduction band and the $H2$ band is the valence band; see sketch of the QW in the inset of Fig. 1(b). The finite maximum in R_{xx} is an indication for the QSHE [4]. Its value is higher than $h/2e^2$ which can be explained by inelastic scattering in large samples [7,8]. This resistance is by an order of magnitude smaller than in samples with comparable size and a 20 meV bulk band gap [7] (see band structure calculations in Fig. 4(c) and in the Supplemental Material [14]). At $V_g = 0$ (ii), both samples are n conducting and sample S1 (S2) has a carrier concentration of $n = 3.7 \times 10^{11}$ cm^{-2} ($n = 4.5 \times 10^{11}$ cm^{-2}) and a mobility of $\mu = 5.6 \times 10^4$ cm^2/Vs ($\mu = 4.6 \times 10^5$ cm^2/Vs). The fact that we can indeed tune the Fermi energy through the bulk band gap is demonstrated by measuring the Hall resistivity ρ_{xy}, shown in Figs. 1(c) and 1(d). Depending on V_g, we find a positive ρ_{xy} caused by negatively charged electrons in (i) and (ii), and a negative ρ_{xy} in (iii) indicating hole transport. At higher magnetic fields, we observe the quantum Hall effect for electrons, and the ρ_{xy} for holes diverges. Quantization in ρ_{xy} for holes occurs at lower temperatures, see Fig. 1(d) at 0.3 K owing to the higher effective mass for holes [2].

III. MAGNETOTRANSPORT AT ROOM TEMPERATURE

We now present magnetotransport at room temperature. At high temperatures we are limited to apply a high $|V_g|$ due to an increase in the leak current through the insulator. In Fig. 2, we show magnetotransport for sample S1 at $T = 300$ K. Applying a gate voltage V_g at $B = 0$, we find that ρ_{xx} increases with decreasing V_g, see inset of Fig. 2(a), indicating that we deplete electrons when decreasing the gate voltage. In Figs. 2(a) and 2(b), we illustrate ρ_{xx} and ρ_{xy} as a function of the magnetic field for various fixed V_g. For all gate voltages, ρ_{xx} displays a pronounced MR and ρ_{xy} shows a strong nonlinear behavior. For positive V_g, ρ_{xx} increases quadratically as a function of B but with decreasing V_g, we find that ρ_{xx} deviates from the quadratic behavior and exhibits a small MR seemingly saturating in higher magnetic fields.

Both observations point towards a system where electrons and holes coexist. Notably, the slope of ρ_{xy} is first positive, indicating a dominant contribution of mobile electrons. With increasing magnetic field, the slope becomes negative due to holes with a higher concentration and lower mobility.

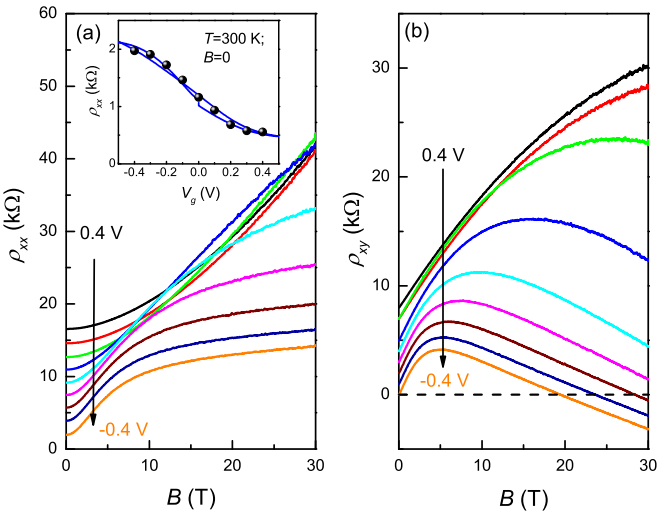

FIG. 2. (Color online) Magnetotransport at room temperature. (a) ρ_{xx} (offset for clarity by 2 kΩ except trace at $V_g = -0.4$ V) and (b) ρ_{xy} (offset for clarity by 1 kΩ except trace at $V_g = -0.4$ V) as a function of B for fixed V_g: for high positive V_g, ρ_{xx} has a quadratic MR accompanied by saturating ρ_{xy}, whereas ρ_{xx} exhibits a transition from quadratic to almost field-independent MR for negative V_g accompanied by a linear decrease in ρ_{xy} at higher fields. Inset: ρ_{xx} as a function of V_g at $B = 0$ [solid line: continuous gate sweep; symbols: $\rho_{xx}(B)$ for a fixed V_g].

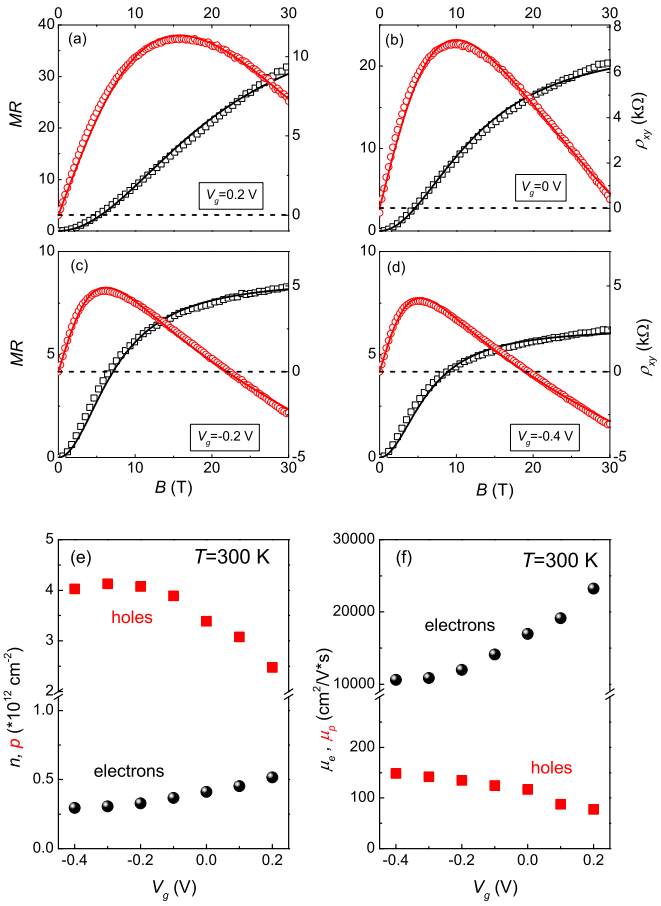

FIG. 3. (Color online) Analysis of room-temperature magnetotransport with a two-carrier Drude model (symbols represent the experimental data, solid lines fits to the model): (a)–(d) MR and ρ_{xy} up to $B = 30$ T for several chosen gate voltages. (e) Charge carrier concentrations and (f) charge carrier mobilities for electrons and holes at different V_g as extracted from the fits. With decreasing gate voltage, the electron (hole) concentration and mobility decreases (increases).

We can extract quantitative information on the charge carrier properties using a semiclassical Drude-model with field-independent electron and hole concentrations and mobilities where we sum up the individual contributions of both electrons and holes to the conductivity tensor $\widehat{\sigma}$

$$\sigma_{xx} = \frac{ne\mu_e}{(1+\mu_e^2B^2)} + \frac{pe\mu_p}{(1+\mu_p^2B^2)}$$
$$\sigma_{xy} = \frac{ne\mu_e^2B}{(1+\mu_e^2B^2)} - \frac{pe\mu_p^2B}{(1+\mu_p^2B^2)} \quad (1)$$

and perform a fit to the experimentally measured resistivity tensor $\widehat{\rho} = \widehat{\sigma}^{-1}$.

The results of the simultaneous fitting of the relative magnetoresistance, defined as $\mathrm{MR} = [\rho_{xx}(B) - \rho_{xx}(0)]/\rho_{xx}(0)$, and the Hall resistance $\rho_{xy}(B)$ at four chosen fixed gate voltages are shown as the solid lines in Figs. 3(a)–3(d). The gate dependencies of the electron and hole concentrations n and p, and the mobilities μ_e and μ_p extracted from the fits, are illustrated in Figs. 3(e) and 3(f). Therefore, transport is governed by an electron band with very mobile carriers, i.e., carriers with a small effective mass, coexisting with a hole band with a large amount of charge carriers with a large effective mass and low mobility.

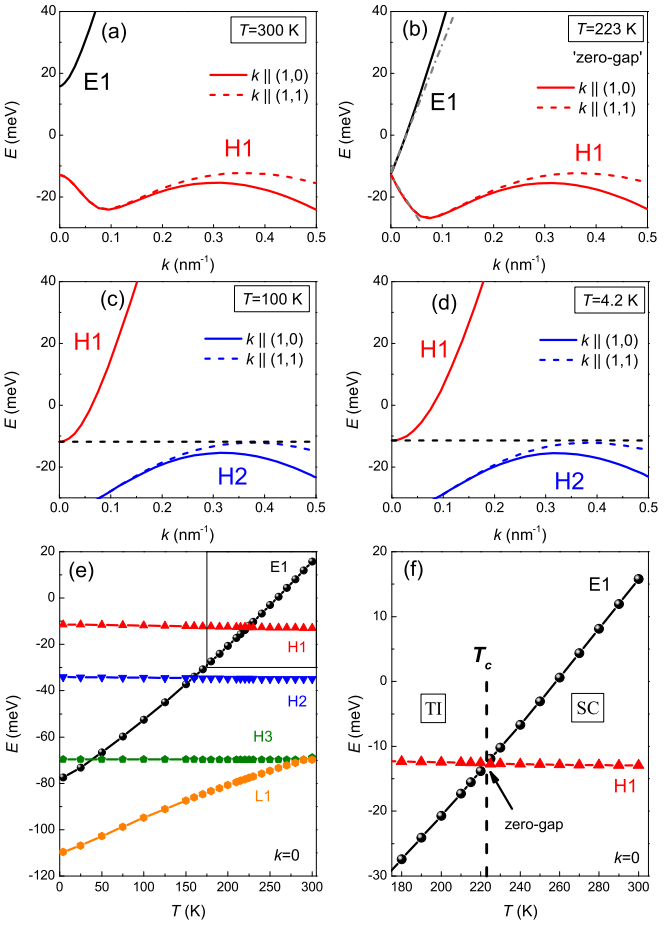

FIG. 4. (Color online) Band structure calculations for sample S1 for $k||(1,0)$ and $k||(1,1)$: (a)–(d) $E(k)$ for (a) at 300 K with a normal BS ($E1 > H1$), (b) at 223 K where the system is a zero-gap semiconductor (dashed-dotted lines show $E \propto k$ for small k where the $E1$ and $H1$ bands touch each other at $k = 0$), (c) at 100 K, and (d) at 4.2 K with an inverted BS. We find an indirect bulk band gap at 4.2 K. (Note that the curvature of the $H1$ band is larger at 100 K compared to 4.2 K). (e) Temperature dependence of the electronlike $E1$, the heavy-hole-like $H1$, $H2$, and $H3$ and the light-hole-like $L1$ subband as a function of temperature at $k = 0$. The $E1$ and $L1$ band decrease with decreasing T. (f) Crossing of $E1$ and $H1$ at T_c: for $T > 223$ K, the system is a normal semiconductor. For $T < 223$ K, we have a QW with an inverted BS and thus, a 2D TI.

IV. TEMPERATURE-DEPENDENT BAND STRUCTURE CALCULATIONS

So far, we have presented that our system is a 2D TI at low temperature whereas magnetotransport can be described within a classical two-carrier model for one electron and one hole band at room temperature as expected for a conventional semiconductor if the thermal energy k_BT is larger than the band gap E_g. This transition can be elucidated by performing temperature-dependent bulk band structure calculations of the QW structures shown for sample S1 in Fig. 4. Additional BS

calculations for sample S2 are illustrated in the Supplemental Material [14]. Our calculations are based on an eight-band $\mathbf{k}\cdot\mathbf{p}$ model in the envelope function approach [15]. The $\mathbf{k}\cdot\mathbf{p}$ model takes into account the temperature dependence of all relevant parameters, in particular the change in the lattice constants of $Hg_{1-x}Cd_xTe$ and the elastic constants C_{11}, C_{12} (bulk modulus) and C_{44} with temperature [16,17]. The elastic constants C_{ij} increase by a few % with decreasing T but the ratios which enter the calculations remain constant. In Figs. 4(a)–4(d), we plot $E(k)$ for the 12 nm thick QW at different temperatures used in our experiment. At 300 K, the gap between the conduction band $E1$ and the valence band $H1$ is $E_g \simeq 26$ meV. With decreasing temperature, the band gap E_g considerably decreases and the 12 nm HgTe QW becomes a zero-gap SC at $T = 223$ K [10], see Fig. 4(b). In this temperature range $E_g \leqslant k_B T$, and transport is still governed by thermally activated charge carriers within the $E1$ and $H1$ bands. Decreasing the temperature further, the BS becomes inverted and the system has an indirect bulk band gap. Thus, the BS calculations demonstrate a transition from a conventional semiconductor with normal band ordering to a 2D TI. At $T = 100$ K, see Fig. 4(c), transport is still dominated by thermally activated charge carriers but now in the $H1$ conduction and the $H2$ valence band since $E_g \leqslant k_B T$. At low temperatures, see Fig. 4(d) for $T = 4.2$ K, $E_g > k_B T$ and thermal activation becomes negligible, and we would observe an infinite resistance in the bulk band gap for a perfectly homogeneous gate potential if our system was not a 2D TI.

In Fig. 4(e), we plot an overview of the temperature dependence of the electron band $E1$, the heavy-hole bands $H1$, $H2$, and $H3$ and the light hole band $L1$ at the Γ point ($k = 0$). As can be seen from the calculation, the system undergoes a transition from a conventional semiconductor to a 2D TI due to the decrease of the $E1$ band in energy, highlighted in Fig. 4(f) where the temperature dependence of $E1$ and $H1$ is illustrated. For $T > 223$ K, our system is a conventional semiconductor with the conduction band $E1$ and the valence band $H1$ with a direct band gap [indirect band gap] for $k||(1,0)$ [$k||(1,1)$].

V. REGIME OF LINEAR MAGNETORESISTANCE

Let us now draw our attention to the intermediate temperature regime where, according to the presented BS calculation, the band order is inverted but transport is still dominated by thermally activated charge carriers. In Fig. 5(a), we plot $\rho_{xx}(T)$ at $V_g = 0$ and observe that ρ_{xx} first increases with decreasing temperature, which is characteristic for a semiconductor with thermally activated carriers. Around 130 K, ρ_{xx} displays a maximum and then starts to decrease with further decreasing temperature before saturating for $T \leqslant 10$ K. This behavior is characteristic for a metallic system with a constant carrier concentration and an increasing mobility with decreasing temperature. In Fig. 5(b), we plot the resistivity ρ_{xx} as a function of V_g at 100, 150, and 204 K. For $T > 100$ K, ρ_{xx} decreases monotonously with increasing V_g. For $T = 100$ K, we observe a maximum in ρ_{xx} which we refer to as the region of charge neutrality.

A particular feature of this intermediate-temperature regime is the emergence of a strong LMR that develops from a classical quadratic low-field MR. In Figs. 5(c) and 5(d) we plot ρ_{xx} and

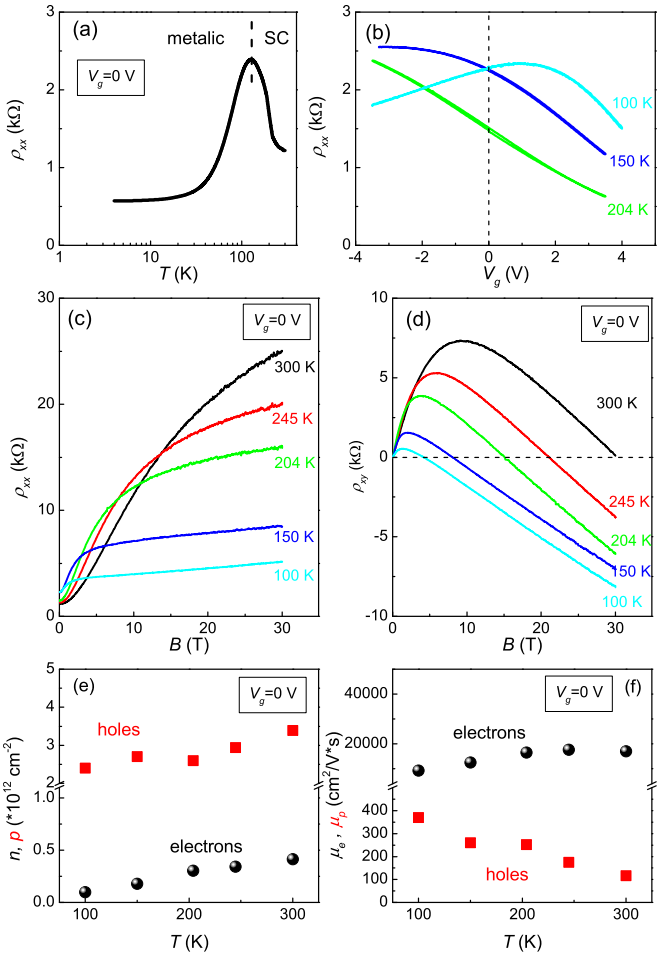

FIG. 5. (Color online) Temperature-dependent magnetotransport: (a) $\rho_{xx}(T)$ at $V_g = 0$ shows a maximum around 130 K, then decreases and saturates with decreasing temperature. (b) ρ_{xx} as a function of V_g at different temperatures. For $T = 100$ K, R_{xx} exhibits a maximum at $V_g = 1$ V which we identify as the CNP. (c) ρ_{xx} and (d) Hall resistivity as a function of B at $V_g = 0$ for 300, 245, 204, 150, and 100 K. For 150 and 100 K, ρ_{xx} exhibits LMR in a wide range of magnetic field. (e) Carrier concentrations and mobilities for electrons and holes as a function of temperature. The dashed lines (dashed-dotted lines) mark the border between two-carrier transport and one-carrier n conduction for $k||(1,0)$ when the thermal energy is smaller than the bulk band gap extracted from BS calculations.

ρ_{xy} at $V_g = 0$ as a function of B for several temperatures. In the temperature range presented in Fig. 5(c), $E_g \leqslant k_B T$ at $V_g = 0$ and magnetotransport is governed by bulk electrons and holes. For high temperatures ($T > 200$ K), we observe a quadratic MR that can be perfectly modeled by a two-carrier Drude model (see also Fig. 3). For lower temperatures, however, we find two different regimes in $\rho_{xx}(B)$: a quadratic MR at low magnetic fields, as expected from the classical two-carrier Drude model, and a LMR at high B. Furthermore, the onset of LMR shifts continuously to lower B with decreasing temperature. Interestingly, at $T = 150$ and 100 K, we observe a wide range of LMR, e.g., from 8 to 30 T at 150 K and 3 to 30 T at 100 K, respectively. The experimentally observed MR can not be described by the classical two-carrier model though the corresponding ρ_{xy} traces indicate that both electrons and

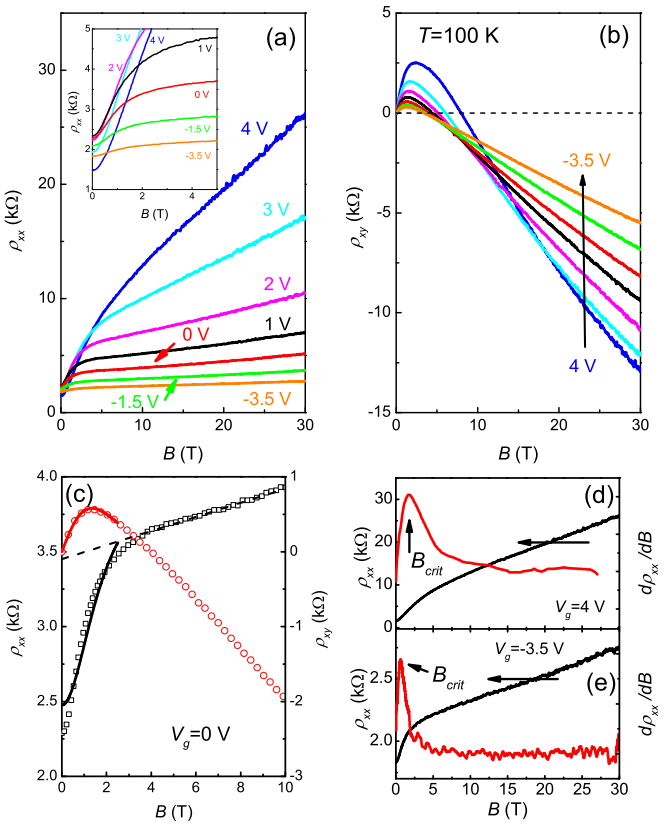

FIG. 6. (Color online) Magnetotransport at $T = 100$ K: (a) ρ_{xx} (inset: low-field behavior of ρ_{xx}) and (b) ρ_{xy} as a function of B for different gate voltages. For all V_g, ρ_{xx} exhibits strong LMR. (c) Applied two-carrier fit model (solid lines), measured ρ_{xx} and ρ_{xy} (open symbols and circles) at $V_g = 0$. (d), (e) The onset of LMR shifts to lower B with decreasing V_g where both ρ_{xx} and $d\rho_{xx}/dB$ are plotted as a function of B for $V_g = 4$ V and $V_g = -3.5$ V, respectively. B_{crit} marks the transition from quadratic MR to LMR.

holes still contribute to the transport. We estimate the electron concentrations from the linear increase of ρ_{xy} at low B and the hole concentration from the slope of ρ_{xy} at high B, and the results are shown in Fig. 5(e). When we decrease the temperature from 300 to 100 K, n and p decrease by approximately a factor of two and 1.5, respectively, which can again be explained by the decrease of thermally exited carriers. We can also estimate the carrier mobilities, by limiting the two-carrier model to the classical regime at low magnetic fields. An example of a two-carrier fit is shown in Fig. 6(c) for $B \leqslant 2.5$ T (solid lines) at 100 K.

As an example for the peculiar MR below T_c when the band structure is inverted, we plot ρ_{xx} and ρ_{xy} in Figs. 6(a) and 6(b) as a function of the magnetic field up to 30 T at different V_g, respectively. For $V_g \geqslant 1$ V, ρ_{xx} exhibits a strong positive MR at low fields that evolves into a strong linear MR with increasing B. For $V_g \leqslant 1$ V, the MR is still positive at low B and becomes linear as the field is increased, see also inset of Fig. 6(a), and the onset of LMR shifts to lower magnetic field with decreasing V_g. The linear dependence of ρ_{xx} and its onset can be clearly illustrated in the first-order derivative $d\rho_{xx}/dB$, as plotted in Fig. 6(d) and (e) as a function of the magnetic field. We define a critical field B_{crit} as the magnetic field corresponding to the maximum in $d\rho_{xx}/dB$, which marks the deviation from a squared dependence in the two-carrier model for low B. For all V_g, ρ_{xy} is first positive due to mobile electrons and becomes negative with increasing B due to the presence of holes.

VI. DISCUSSION

From the above bulk BS calculations we see that temperature induces a transition from a normal state to a topologically nontrivial state in HgTe QWs. With decreasing temperature ($T > T_c$), the gap closes, see Fig. 4(e). The conduction band exhibits a significant dependence on k, yielding a small effective mass $0.015\ m_e < m^* < 0.04\ m_e$ [2,15,16] for our QW. In contrast, the valence band is more flat pointing to a much higher effective mass ($m^* \simeq 0.2\ m_e$ [16]). As demonstrated in Fig. 4(f), the transition from normal to inverted band order occurs at $T_c = 223$ K. Since the thermal energy is larger than E_g, magnetotransport is dominated by bulk electrons and holes due to the small bulk band gap above and below T_c. Thus, this transition does not occur abruptly in magnetotransport as demonstrated by our experimental data in Figs. 5 and 6. However, as presented in Fig. 6(c), the classical two-carrier model fails to describe the observed MR for $B > B_{crit}$. Moreover, the peculiar MR occurs if electrons and holes with a considerable difference in carrier concentration and mobility coexist. The fact that our bulk band structure is inverted for $T < 223$ K implies that transport can also take place in helical edge states with a linear dispersion in the bulk band gap [4–7].

The observation of LMR has been reported in various systems such as bulk narrow-band gap semiconductors [18,19] and semimetals [20] as well as recently in TIs [21]. In fact, the occurrence of a strong LMR has been ascribed to surface states in three-dimensional TIs [22]. In a 2D TI (HgTe QW), LMR has been also found at low magnetic field and low temperature when the chemical potential moves through the bulk gap [23]. In contrast, since $k_B T > E_g$, LMR in our system is governed by mobile bulk electrons with low density and less mobile holes with high carrier concentration and helical edge states. From V_g-dependent measurements we found that the onset B_{crit} of LMR shifts to lower B with increasing carrier concentration of holes.

Theoretical models have also addressed the appearance of LMR [24,25]. The classical percolation model by Parish and Littlewood [24] for a nonsaturating LMR due to distorted current paths caused by disorder-induced inhomogeneities in the electron mobility cannot be applied to our system since our MBE grown samples do not show strong fluctuations in μ, and it does not explain the transition from classical MR to LMR with increasing magnetic field. The quantum model, that has been proposed by Abrikosov [25], is valid for systems with a gapless linear dispersion spectrum when only the lowest Landau level (LL) remains occupied. Moreover, the energy difference between the lowest LL E_0 and the first LL E_1 should be much larger than E_F and $k_B T$. We reach the quantum limit for one type of charge carriers, e.g., at $V_g = 0$ for $T = 100$ K, since $E_1 - E_0 > E_F > k_B T$, however, the LMR in our 2D system occurs in the presence of two types of charge carriers in the bulk and charge carriers in the helical edge states in

contrast to the three-dimensional model for one type of charge carrier proposed by Abrikosov [25].

Recently, MR has been theoretically investigated in two-component systems such as narrow-band semiconductors or semimetals at high temperatures [26]. For equal carrier concentrations of electrons and holes, a nonsaturating LMR has been predicted to occur in finite size at charge neutrality due to the interplay between bulk and edge contributions. At room temperature, our data in Fig. 2 shows qualitatively the expected behavior for ρ_{xx} and ρ_{xy} as proposed and illustrated in Ref. [26] for broken electron-hole symmetry. Yet we have shown that both ρ_{xx} and ρ_{xy} can also be explained within the classical two-carrier model without any contribution due to a quasiparticle density that develops near the sample edges. A satisfactory theoretical explanation of the origin of LMR for $T < T_c$ and $B > B_{crit}$ that also addresses the role of helical edge states at high temperature remains open and is certainly challenging for theoretical models in the future.

VII. CONCLUSION

We have demonstrated in bulk band structure calculations on HgTe QWs that temperature induces a transition from a semiconductor at room temperature to a TI at low temperature. Experimentally, we can distinguish between three regimes in magnetotransport: (i) transport of coexisting electrons and holes that can be described within a classical two-carrier model at room temperature, (ii) the appearance of a strong LMR for $B > B_{crit}$ and $T < T_c$ where electrons and holes still coexist, and (iii) the regime of quantized transport ($\hbar\omega_c > k_B T$) at low temperature where we are also in the regime of the QSHE. We note that apart from inverted HgTe QWs, the only other system known to be a 2D TI is the InAs/GaSb hybrid system [27] that has been investigated at low temperature [8,9,28]. Temperature-dependent magnetotransport experiments could demonstrate whether the MR effects are unique in inverted HgTe QWs due to their bulk band structure or are a fundamental property of 2D topological insulators.

ACKNOWLEDGMENTS

This work has been performed at the HFML-RU/FOM member of the European Magnetic Field Laboratory (EMFL) and has been supported by EuroMagNET II under EU Contract No. 228043, by the DARPA MESO project through the Contract No. N66001-11-1-4105, by the German Research Foundation (DFG Grant No. HA5893/4-1 within SPP 1666, the Leibniz Program, and DFG-JST joint research project ´Topological Electronics´), and the EU ERC-AG program (Project 3-TOP). S.W. is financially supported by a VENI grant of the Nederlandse Organisatie voor Wetenschappelijk Onderzoek (NWO).

[1] J. Chu and A. Sher, *Physics and Properties of Narrow Gap Semiconductors* (Springer, New York, 2010).

[2] A. Pfeuffer-Jeschke, F. Goschenhofer, S. J. Cheng, V. Latussek, J. Gerschütz, C. R. Becker, R. R. Gerhardts, and G. Landwehr, Cyclotron masses of asymmetrically doped HgTe quantum wells, Physica B **256-258**, 486 (1998).

[3] M. Schultz, U. Merkt, A. Sonntag, U. Rössler, R. Winkler, T. Colin, P. Helgesen, T. Skauli, and S. Løvold, Crossing of conduction- and valence-subband Landau levels in an inverted HgTe/CdTe quantum well, Phys. Rev. B **57**, 14772 (1998).

[4] B. A. Bernevig, T. L. Hughes, and S. C. Zhang, Quantum spin Hall effect and topological phase transition in HgTe quantum wells, Science **314**, 1757 (2006).

[5] M. Z. Hasan and C. L. Kane, Topological insulators, Rev. Mod. Phys. **82**, 3045 (2010).

[6] X.-L. Qi and S. C. Zhang, Topological insulators and superconductors, Rev. Mod. Phys. **83**, 1057 (2011).

[7] M. König, S. Wiedmann, C. Brüne, A. Roth, H. Buhmann, L. W. Molenkamp, X.-L. Qi, and S.-C. Zhang, Quantum spin Hall insulator state in HgTe quantum wells, Science **318**, 766 (2007).

[8] L. Du, I. Knez, G. Sullivan, and R. R. Du, Robust Helical edge transport in gated InAs/GaSb bilayers, Phys. Rev. Lett. **114**, 096802 (2015).

[9] K. Suzuki, Y. Harada, K. Onomitsu, and K. Muraki, Edge channel transport in the InAs/GaSb topological insulating phase, Phys. Rev. B **87**, 235311 (2013).

[10] A. Roth, C. Brüne, H. Buhmann, L. W. Molenkamp, J. Maciejko, X.-L. Qi, S.-C. Zhang, Nonlocal transport in the quantum spin hall state, Science **325**, 294 (2009).

[11] C. Brüne, A. Roth, H. Buhmann, E. M. Hankiewicz, L. W. Molenkamp, J. Maciejko, X.-L. Qi, and S.-C. Zhang, Spin polarization of the quantum spin Hall edge states, Nat. Phys. **8**, 486 (2012).

[12] B. Büttner, C. X. Liu, G. Tkachov, E. G. Novik, C. Brüne, H. Buhmann, E. M. Hankiewicz, P. Recher, B. Trauzettel, S. C. Zhang, and L. W. Molenkamp, Single valley Dirac fermions in zero-gap HgTe quantum wells, Nat. Phys. **7**, 418 (2011).

[13] Z. D. Kvon, E. B. Olshanetsky, D. A. Kozlov, N. N. Mikhailov, and S. A. Dvoretskii, Two-dimensional electron-hole system in a HgTe-based quantum well, JETP Lett. **87**, Issue 9 502 (2008).

[14] See Supplemental Material at http://link.aps.org/supplemental/10.1103/PhysRevB.91.205311 for sample description, additional magnetoresistance measurements and band structure calculations for sample S2.

[15] E. G. Novik, A. Pfeuffer-Jeschke, T. Jungwirth, V. Latussek, C. R. Becker, G. Landwehr, H. Buhmann, and L. W. Molenkamp, Band structure of semimagnetic $Hg_{1-x}Mn_xTe$ quantum wells, Phys. Rev. B **72**, 035321 (2005).

[16] A. Pfeuffer-Jeschke, *Dissertation*, University of Würzburg (2007).

[17] *Mercury Cadmium Telluride - Growth, Properties and Applications*, edited by Peter Capper and James Garland (John Wiley & Sons Ltd., The Atrium, Southern Gate, Chichester, 2011).

[18] W. R. Branford, A. Husmann, S. A. Solin, S. K. Clowes, T. Zhang, Y. V. Bugoslavsky, and L. F. Cohen, Geometric manipulation of the high-field linear magnetoresistance in InSb epilayers on GaAs (001), Appl. Phys. Lett. **86**, 202116 (2005).

[19] J. Hu and T. F. Rosenbaum, Classical and quantum routes to linear magnetoresistance, Nat. Mater. **7**, 697 (2008).

[20] R. Xu, A. Husmann, T. F. Rosenbaum, M.-L. Saboungi, J. E. Enderby, and P. B. Littlewood, Large magnetoresistance in non-magnetic silver chalcogenides, Nature (London) **390**, 57 (1997).

[21] W. Zhang, R. Yu, W. Feng, Y. Yao, H. Weng, X. Dai, and Z. Fang, Topological aspect and quantum magneto-resistance of $\beta - Ag_2Te$, Phys. Rev. Lett. **106**, 156808 (2011).

[22] M. Veldhorst, M. Snelder, M. Hoek, C. G. Molenaar, D. P. Leusink, A. A. Golubov, H. Hilgenkamp, and A. Brinkman, Magnetotransport and induced superconductivity in Bi based three-dimensional topological insulators, Phys. Status Solidi RRL **7**, 26 (2013).

[23] G. M. Gusev, E. B. Olshanetsky, Z. D. Kvon, N. N. Mikhailov, and S. A. Dvoretsky, Linear magnetoresistance in HgTe quantum wells, Phys. Rev. B **87**, 081311(R) (2013).

[24] M. M. Parish and P. B. Littlewood, Non-saturating magnetoresistance in heavily disordered semiconductors, Nature (London) **426**, 162 (2003).

[25] A. A. Abrikosov, Quantum magnetoresistance, Phys. Rev. B **58**, 2788 (1998).

[26] P. S. Alekseev, A. P. Dmitriev, I. V. Gornyi, V. Yu. Kachorovskii, B. N. Narozhny, M. Schuett, and M. Titov, Magnetoresistance in two-component systems, Phys. Rev. Lett. **114**, 156601 (2015).

[27] C. Liu, T. L. Hughes, X. L. Qi, K. Wang, and S. C. Zhang, Quantum Spin Hall Effect in Inverted Type-II Semiconductors, Phys. Rev. Lett. **100**, 236601 (2008).

[28] I. Knez, R. R. Du, and G. Sullivan, Evidence for helical edge modes in inverted InAs/GaSb Quantum Wells, Phys. Rev. Lett. **107**, 136603 (2011).